High-resolution angle-resolved photoemission studies of quasiparticle dynamics in graphite

C. S. Leem, Chul Kim, S. R. Park, Min-Kook Kim, Hyoung Joon Choi, and C. Kim*
Institute of Physics and Applied Physics, Yonsei University, Seoul, Korea 120–749

B. J. Kim
School of Physics and Center for Strongly Correlated Materials Research, Seoul National University, Seoul, Korea 151–742

S. Johnston
Department of Photon Science, Stanford Linear Accelerator Center, Stanford University, Menlo Park, California 94025, USA and Department of Physics and Astronomy, University of Waterloo, Waterloo, Ontario, Canada N2L 3G1

T. Devereaux
Department of Photon Science, Stanford Linear Accelerator Center, Stanford University, Menlo Park, California 94025, USA

T. Ohta, A. Bostwick, and E. Rotenberg
Advanced Light Source, Lawrence Berkeley National Laboratory, Berkeley, California 94720, USA
(Received 11 December 2008; revised manuscript received 21 February 2009; published 30 March 2009)

We obtained the spectral function of the graphite *H* point using high-resolution angle-resolved photoelectron spectroscopy (ARPES). The extracted width of the spectral function (inverse of the photohole lifetime) near the *H* point is approximately proportional to the energy as expected from the linearly increasing density of states (DOS) near the Fermi energy. This is well accounted for by our electron-phonon coupling theory considering the peculiar electronic DOS near the Fermi level. We also investigated the temperature dependence of the peak widths both experimentally and theoretically. The upper bound for the electron-phonon coupling parameter is 0.23, nearly the same value as previously reported at the *K* point. Our analysis of temperature-dependent ARPES data at *K* shows that the energy of a phonon mode of graphite has a much higher energy scale than 125 K, which is dominant in electron-phonon coupling.

DOI: 10.1103/PhysRevB.79.125438 PACS number(s): 81.05.Uw, 63.20.kk, 73.20.At, 79.60.−i

I. INTRODUCTION

Fermi-liquid theory[1] (FLT) is thought to be one of the most successful theories for describing the behaviors of electrons in solids, especially electrons near the Fermi energy in metals at low temperature. The success of the FLT in metallic systems naturally raises an issue on how far the FLT scheme can be applied to other condensed-matter systems. Related to this question, there is a long-standing controversy on whether electrons in graphite, a two-dimensional (2D) semimetallic system, can be described within the FLT scheme or not. According to FLT, the lifetime of an electron due to electron-electron interactions is inversely proportional to the square of the binding energy. Therefore, measurement of the lifetime as a function of the binding energy of an electron would be a direct test of the validity of FLT in graphite.

Experimental results do not seem to show evidence of Fermi-liquid behavior of electrons in graphite.[2] In fact, the inverse lifetime measured by two-photon photoemission (2PPE) experiments conducted on natural single-crystal graphite and highly oriented pyrolytic graphite (HOPG) appears to increase linearly as a function of the binding energy.[3] The observed peculiar behavior in the energy dependence of the inverse lifetime was discussed in terms of the peculiar dispersion of plasmon[2] or electron-electron interaction in combination with the band structure of graphite.[4,5]

However, electron-phonon coupling (EPC), one of the most fundamental interactions in solids, has not been considered in the discussion. On the theoretical side, very little work can be found on the EPC in semimetals even though it has been well developed and widely studied in metallic systems.[6] Only very recently have some theoretical models for graphene appeared.[7–9] On the experimental side, electron lifetime was measured only for the energies larger than the maximum phonon energy of graphite (~200 meV) (Refs. 10–12) in the 2PPE experiments.[2,3] Therefore, to address the lifetime issue due to EPC in graphite, one may need two requirements. First, the experimental data must show the lifetime of quasiparticles sufficiently close to the Fermi energy, less than the maximum phonon energy of graphite. Second, a proper model that considers the electron-phonon interaction contribution to the quasiparticle decay should be developed. In regards to the second point, models developed for metals have been used in the analysis of angle-resolved photoemission (ARPES) data on graphite due to the lack of theoretical EPC models for semimetals.[13]

To address the issue of the quasiparticle dynamics and EPC in graphite, we performed high-resolution ARPES experiments on high-quality natural single crystal and developed a theoretical model that considers the linear density of states (DOS) near the Fermi energy.[14] Our previous work was performed near the *K* point and showed a relatively small EPC constant of $\lambda = 0.20$. To extend our previous work, we have obtained high-resolution ARPES data from the *H* point to determine if it also has a small EPC constant. In addition, we have also performed temperature-dependent studies near the *K* point. The temperature-dependent data are

compared with a theoretical model that fully considers the graphite DOS. Properly extracted peak widths are well understood within our EPC model with a linear DOS near the Fermi energy and show a small EPC constant of less than 0.23.

II. THEORY

We first consider the theoretical side of the quasiparticle dynamics in graphite. In this section, we discuss possible decay channels for quasiparticles in graphite. First, it will be discussed how the lifetime of quasiparticles in graphite can be affected by EPC. We will formulate the self-energy of quasiparticles based on the linear DOS of graphite, for zero temperature in Sec. II A 1 and for a finite temperature in Sec. II A 2. The latter is to establish the foundation for estimating the EPC constant through temperature-dependent studies. Second, we will discuss other decay channels such as electron-electron scattering, electron-plasmon scattering, and impurity and defect scattering. Through these discussions, we wish to establish that the dominant scattering mechanism for quasiparticles in graphite comes from the EPC.

A. Electron-phonon coupling in graphite

Electron-phonon interaction theory is an extensively studied subject in condensed-matter physics. The importance of its role is highlighted in the theory for conventional superconductors, i.e., the BCS theory. Even though a general theory should be applicable to any system, specific and more applicable models have been developed for metallic systems. However, a key assumption used for metallic systems, constant DOS near the Fermi level, is not valid for semimetals and insulators. To the best of our knowledge, EPCs in semimetals and insulators have not been thoroughly studied theoretically (probably due to lack of interest). With recent developments in graphene and graphite related research,[7,8,15] EPC in semimetals has become more important. Therefore, we need a model to evaluate the EPC constant in graphite.

To understand the EPC in graphite, one should consider its characteristic band structure near the Fermi level. Figure 1(a) shows the crystal structure of graphite. Graphite has a layered structure and the stacking order is $ABAB\cdots$. In each layer, carbon atoms form strong σ bonds produced by sp^2 hybridization, while the out-of-plane p_z orbitals form π bonds. Figure 1(b) depicts the first Brillouin zone (BZ) and high-symmetry points of graphite in reciprocal space. The calculated electronic band dispersion of graphite along the high-symmetry line, *A*-*L*-*H*-*A*, is plotted in Fig. 1(c). The band dispersion within ± 1 eV near the H point is almost linear. A three-dimensional view of the band dispersion is shown in Fig. 1(d). The point at which the two cones meet each other is at the Fermi energy and is called the Dirac point. This band structure yields a DOS which increases linearly with binding energy (linear DOS). Numerous studies of the band structure of graphite can be found from both theoretical[16–20] and experimental sides.[21–34]

The electron-phonon coupling theory in graphite should be considered within this characteristic linear DOS. To understand the electron-phonon coupling in graphite, one needs to get the real or the imaginary part of the self-energy. If one approaches electron-phonon coupling through the real part of the self-energy, one has to confront a task of finding the bare band. The bare band of graphite is not linear and hence is much harder to guess in comparison with metallic systems. Even though it was argued that the experimentally measured band structure at H is linear,[33] our results show that the dispersion is not linear and has some parabolic character near the Fermi energy. Therefore, we chose to use the imaginary part in the analysis. Note that the real part of the self-energy can be obtained by Hilbert transforming the imaginary part. Figure 2(a) shows the Feynman diagram[35] for the lowest-order EPC under consideration. Our model considers only this lowest-order EPC in this section. One can describe the many-body effects on quasiparticles using a self-energy scheme. The imaginary part of the self-energy is proportional to the scattering rate of quasiparticles. Here, we present the EPC process for zero- ($T=0$) and finite-temperature cases ($T\neq 0$) separately.

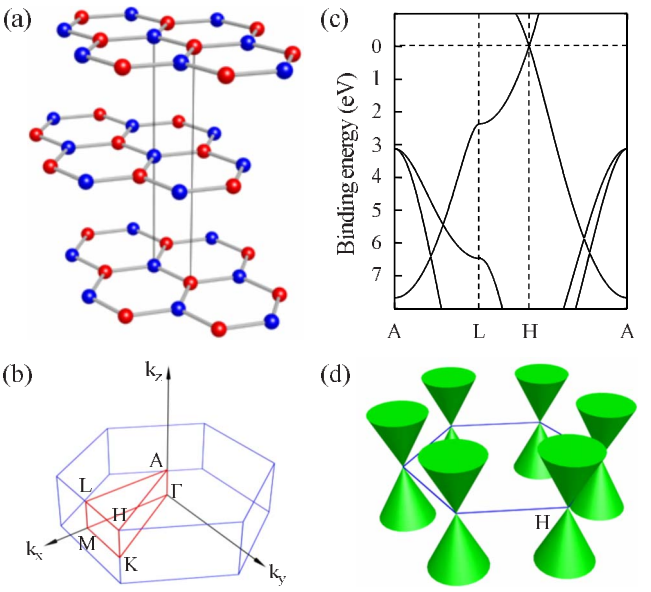

FIG. 1. (Color online) (a) The structure of graphite. Spheres are carbon atoms. Graphite shows a layered structure, which has a stacking order of $ABAB\cdots$. (b) First Brillouin zone (BZ) of graphite. The symbols represent high-symmetry points. (c) Calculated electronic band structure along *A*-*L*-*H*-*A*. (d) Approximated band structure. Each corner of hexagon is H point and z direction is energy.

1. Zero-temperature case

The Hamiltonian of EPC interaction can be written as

$$H_{\mathrm{ep}} = \sum_{i,\sigma,\nu} g_\nu c^\dagger_{k+q,\sigma} c_{k,\sigma} (b^\dagger_{q,\nu} + b_{-q,\nu}), \tag{1}$$

where $c^\dagger_{k,\sigma}$ ($c_{k,\sigma}$) creates (annihilates) an electron with spin σ and momentum k, while $b^\dagger_q$ (b_q) creates (annihilates) a phonon ν with momentum q. The scattering amplitude g is taken to be energy and momentum independent. The $b^\dagger_{q,\nu}$ term is for the phonon emission process and the $b_{-q,\nu}$ term is for

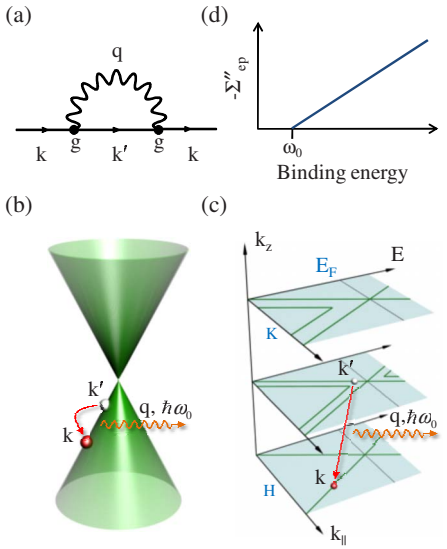

FIG. 2. (Color online) (a) The lowest-order Feynman diagram for EPC. g is electron-phonon coupling constant. k and k' are crystal momenta of holes. q is momentum of phonon. (b) Schematic diagram of the EPC process as shown in panel (a). Photohole k makes a transition to k' emitting phonon of q. $\hbar\omega_0$ is the emitted phonon energy. (c) Schematic diagram for scattering in k_z direction. (d) The imaginary part of the self-energy vs binding energy predicted by our qualitative theory (see the text).

phonon absorption. Then the imaginary part of the self-energy is defined as a convolution over the density of states:[36]

$$\Sigma''_{ep}(\omega) = \sum_{\nu} -g_\nu^2\pi\{\mathcal{D}(\omega-\omega_\nu)[f(\omega_\nu-\omega)+b(\omega_\nu)] + \mathcal{D}(\omega+\omega_\nu)[f(\omega_\nu+\omega)+b(\omega_\nu)]\}, \quad (2)$$

where $\mathcal{D}$ is the electronic DOS and ω_ν is the energy of a phonon ν. f and b are Fermi-Dirac and Bose-Einstein distributions, respectively. Since the electron-phonon interaction does not alter the spin of a conduction electron, spin index σ is suppressed to consider only one spin direction.

If we assume an Einstein phonon with an energy of ω_0 and momentum-independent coupling amplitude g, Eq. (2) becomes

$$\Sigma''_{ep}(\omega) = -g^2\pi\{\mathcal{D}(\omega-\omega_0)[f(\omega_0-\omega)+b(\omega_0)] + \mathcal{D}(\omega+\omega_0)[f(\omega_0+\omega)+b(\omega_0)]\}. \quad (3)$$

For the zero-temperature case, Fermi-Dirac function can be replaced by step function and the Bose factor is zero in Eq. (3). Then, Eq. (3) can be written as

$$\Sigma''_{ep}(\omega, T=0) = -g^2\pi[\mathcal{D}(\omega-\omega_0)\Theta(\omega-\omega_0) + \mathcal{D}(\omega+\omega_0)\Theta(-\omega-\omega_0)], \quad (4)$$

where Θ is a step function, $\Theta(x)=0(x<0)$ and $\Theta(x)=1(x\geq 0)$.

We assume a conical band structure with the Fermi energy at the apex of the cone. There is another conical band above the Fermi energy which is unoccupied, and these two conical bands form a Dirac-cone-like band structure as shown in Fig. 2(b). If a photohole with momentum $\mathbf{k}$ (filled circle) is created by a photon as shown in Fig. 2(b), it can be filled by an electron with energy of $\omega_{k'}=\omega_k-\omega_0$ and momentum $\mathbf{k}'=\mathbf{k}-\mathbf{q}$ (empty circle), where $\mathbf{q}$ is the phonon momentum. The scattering rate is proportional to the number of such $\mathbf{k}'$ states and, thus, the DOS at $\omega_k-\omega_0$. Note that if the binding energy of the photohole is smaller than the phonon energy ω_0, the scattering cannot occur because there are no electrons with sufficient energy to emit a phonon with energy ω_0. Therefore, the imaginary part of the self-energy of the photohole as a function of the binding energy is proportional to $\mathcal{D}(\omega_k-\omega_0)$ and looks like the schematic shown in Fig. 2(d). Note that it is also possible that a phonon may scatter a photohole in the k_z direction as shown in Fig. 2(c). The outcome is not much affected by the c-axis scattering due to the weak dispersion of the π band along the k_z direction.

Once Σ'' is obtained, one can obtain the real part of self-energy Σ'_{ep} by Hilbert transforming Σ''. The electron-phonon coupling parameter λ is defined as

$$\lambda = -\left.\frac{\partial\Sigma'_{ep}(\omega)}{\partial\omega}\right|_{\omega=0}. \quad (5)$$

At the K point, the bonding bands (BBs) and antibonding bands are split because of the interlayer interaction of graphite.[37] Considering the small interband scattering of the photohole by a phonon between bonding bands and nonbonding bands (NBs) at the K point, the above self-energy can be extended to the double-band case at K. This double-band case was investigated in our previous work.[14]

We also note that Σ'_{ep} is not affected seriously by the detailed shape of Σ''_{ep} near $\omega=0$ because Σ''_{ep} increases linearly. This aspect was considered in calculating Σ''_{ep} for K and H points.[9] It was argued that Σ''_{ep} is somewhat different at K and H because the band structure at K is parabolic near the Fermi level, while that at H is linear. Meanwhile some difference between K and H certainly exists that affects the detailed shape of Σ''_{ep} near the Fermi energy; the effect on the EPC constant λ should be negligible because the contribution comes mostly from the high binding energy side.

2. Finite-temperature case

We now move on to the finite-temperature case. In the case of metals, there is an easy way to extract the EPC constant λ from temperature-dependent data through a simple formula.[6,38] The formula is derived under the assumption that the electronic DOS near the Fermi energy is constant, which is not the case for graphite. Here, we investigate the temperature dependence of Σ''_{ep} theoretically to determine if one can easily extract λ from the temperature-dependent data. It turns out that a simple formula such as the one for metals cannot be formulated. However, we show some possibility of estimating EPCs from the temperature-dependent data.

The imaginary part of the self-energy by electron-phonon coupling at finite temperature was shown in Eq. (3) of Sec. II A 1. Note that for the high phonon frequency (for example, A'_1 or E_{2g} mode in graphite) the Bose factors can be neglected for the temperature range over which we per-

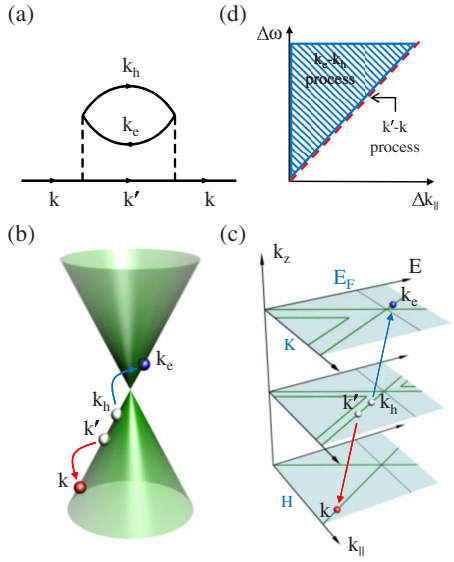

FIG. 3. (Color online) (a) The Feynman diagram for the lowest order for electron-hole pair creation process. Photohole k makes a transition to a hole k', and an electron k_e and a hole k_h are created, conserving momenta and energy. (b) Schematic diagram for electron-hole pair creation in phase space. (c) Schematic diagram for electron-hole pair creation considering the scattering along k_z direction. (d) Hatched area represents the possible Δk and $\Delta\omega$ for electron-hole pair creation. Dashed line represents the possible Δk and $\Delta\omega$ for photohole transition. These two areas slightly touch each other at the line; therefore there is no available phase space.

formed our experiments (10–225 K). We consider not only these high-energy phonons but also low-energy phonons. Unfortunately, the temperature dependence of Σ''_{ep} in Eq. (7) cannot be reduced to a simple form as the one for a metal,[6] and extracting the λ from the temperature dependence of Σ''_{ep} is not a straightforward task. However, one can still obtain information from the temperature-dependent data. If the low-frequency phonon mode participates in EPC, the temperature dependence of Σ''_{ep} near the Fermi level should be strong, while the high-frequency phonon modes should contribute little to the temperature dependence. In addition, the Bose factor in Eq. (3) is not negligible and Σ''_{ep} will show clear differences at different temperatures. Therefore, once the g value is known, one can roughly identify which phonon mode contributes the most to EPC by fitting the temperature-dependent data.

B. Electron-electron interaction in graphite

Electron-electron interactions can also affect the quasiparticle lifetime or the imaginary part of the self-energy. We consider the lowest-order scattering in electron-electron interaction occurring via electron-hole pair creation. The Feynman diagram for this scattering process is shown in Fig. 3(a). When the photohole of crystal momentum $\mathbf{k}$ is created, the hole makes the transition to $\mathbf{k}'$ by creating another hole, $\mathbf{k_h}$, and electron, $\mathbf{k_e}$. Figure 3(b) shows this electron-hole pair creation process in the E-k phase space. From the figure, one can see that the electron-hole pair creation process is negligible under the linear DOS of graphite near the Fermi energy. Let us consider the available phase space for electron-hole pair creation in Fig. 3(b). If we plot the energy difference ($\Delta\omega=\omega_{k'}-\omega_k$, where $\omega_{k'}$ and ω_k are the energies of the holes with $\mathbf{k}'$ and $\mathbf{k}$, respectively) as a function of momentum difference ($\Delta\mathbf{k}=\mathbf{k}'-\mathbf{k}$), the possible transitions occupy the area below the dashed line in Fig. 3(d). In a similar way, one can find that the electron-hole creation process occupies the hatched area in Fig. 3(d). Photohole decay through the electron-hole pair creation can occur only when the two conditions are met, that is, where the phase spaces for the two processes overlap. They overlap only on the dashed line as can be seen in Fig. 3(d). Therefore, the available phase-space volume for the decay through electron-hole pair creation is zero. Note that this is true only near the Fermi energy where the band structure can be approximated by Dirac cones. For the photoholes at higher binding energies, the available phase-space volume becomes nonzero. This fact was previously pointed out by Moos *et al.*[3] If we limit our discussion to the low-energy dynamics in graphite, the effect of the electron-electron interaction can be neglected.

C. Other scattering mechanisms

There are other mechanisms in graphite that may contribute to the quasiparticle scattering such as plasmons, impurities, and defects. Xu *et al.*[2] suggested that plasmons may be the main source for the quasiparticle scattering in graphite. However, Spataru *et al.*[5] showed that electron-hole pair creation should be a more dominant mechanism than electron-plasmon interactions for electron scattering in graphite. Since we have shown in our earlier work[14] that electron-phonon interaction is more dominant than electron-hole pair creation based on a phase-space argument, we may conclude that electron-plasmon interaction is much weaker than electron-phonon coupling and thus may be neglected. Impurity and defect scattering can also contribute to the scattering rate in graphite. These scattering mechanisms also have a rate that is proportional to the electronic DOS as in the electron-phonon coupling case and thus increase the slope for the imaginary part of the self-energy. This fact tells us that if one wants to study the electron-phonon coupling, the experiment should be conducted on clean single-crystalline graphite. In our case, we used natural graphite single crystals which have superior quality to crystals used in other experiments. As a result, we did not observe any defect-related states[13,34] and we therefore believe that defect or impurity scattering is minimal.

In short, among all the possible scattering mechanisms we have considered, electron-phonon coupling should be strongest and dominant because other mechanisms are weak due to lack of phase space (electron-hole pair) or high quality of the crystal (low impurity/defect levels).

III. EXPERIMENT

ARPES experiments were performed at Beamline 7.0.1 of the Advanced Light Source. We used very high quality natural graphite single crystals with sizes larger than $\approx$1 cm.

Samples were cleaved repeatedly *ex situ* by a taping method until a flat surface without large flakes was obtained. Samples were subsequently introduced to the ultrahigh vacuum chamber and annealed at 900 °C for 30 min in a vacuum better than 6.0×10^{-10} Torr to clean the surface. The energy resolution was ≈40 meV. The chamber pressure was better than 5.0×10^{-11} Torr during the measurements. We found that the typical size of the flat regions without flakes was smaller than 200 μm. Therefore, we exploited the small beam spot (≈50 μm) to probe the flat region.

We took $k_z=H$ data at 20 K with a photon energy of 103.4 eV to obtain the electron-phonon coupling by analyzing the peak width as a function of the binding energy. This is essentially the same as what we reported earlier[14] but at the *H* point. In addition, we performed the temperature-dependent experiment at the *K* point with a photon energy of 85 eV. ARPES data were taken at 25, 75, 125, 175, and 225 K. We started measuring at 225 K and lowered the temperature. After having measured at 25 K, we annealed the sample again for ≈30 s at ≈900 °C and measured again. Comparison of the data before and after annealing showed essentially no difference, indicating that there was no surface contamination during the measurement. For comparison, graphene data were also taken at the *K* point. The graphene sample was epitaxially grown on 6*H*-SiC *in situ* as reported elsewhere.[39] Electronic band-structure calculation was done by using the SIESTA code based on the pseudopotential method.

IV. RESULTS AND DISCUSSION

A. Low-temperature case

Figure 4(a) shows measured the ARPES spectral function along the *L*-*H*-*A* symmetry line. The NB and BB are degenerate at the *H* point, whereas they are split at the *K* point. We could identify only one peak in the energy distribution curves (EDCs) and momentum distribution curves (MDCs). We also took data with different photon energies to ensure that we were really at the *H* point. The electronic band near the Fermi energy shows a linear dispersion as predicted in the band calculation in Fig. 1(c). However, we also note that the band dispersion very near the Fermi level shows some parabolic component contrary to what is expected from the theory. This could be due to k_z broadening caused by the finite escape depth. We also note that there are no evidence for defect-induced states that were reported earlier.[32] This indicates that our natural graphite single crystals are of very high quality. Almost negligible background of our data even at high binding energy further supports the high quality of our sample. This means that the defect or impurity contribution to the scattering rate is very small and we may only consider the electron-phonon coupling effect.

Figure 4(b) shows the EDC from the *k* point indicated by the arrow in panel (a). The line shape of the EDC is very asymmetric. As was the case for the *K* data,[14] we can understand this asymmetry as follows. Though we tuned the photon energy to probe the *H* point of graphite, the finite escape depth of the photoelectron yields an uncertainty in k_z, $\Delta k_z = 1/\mu$, where μ is the escape depth. Therefore, there is a contribution from other k_z values, which is illustrated in Fig.

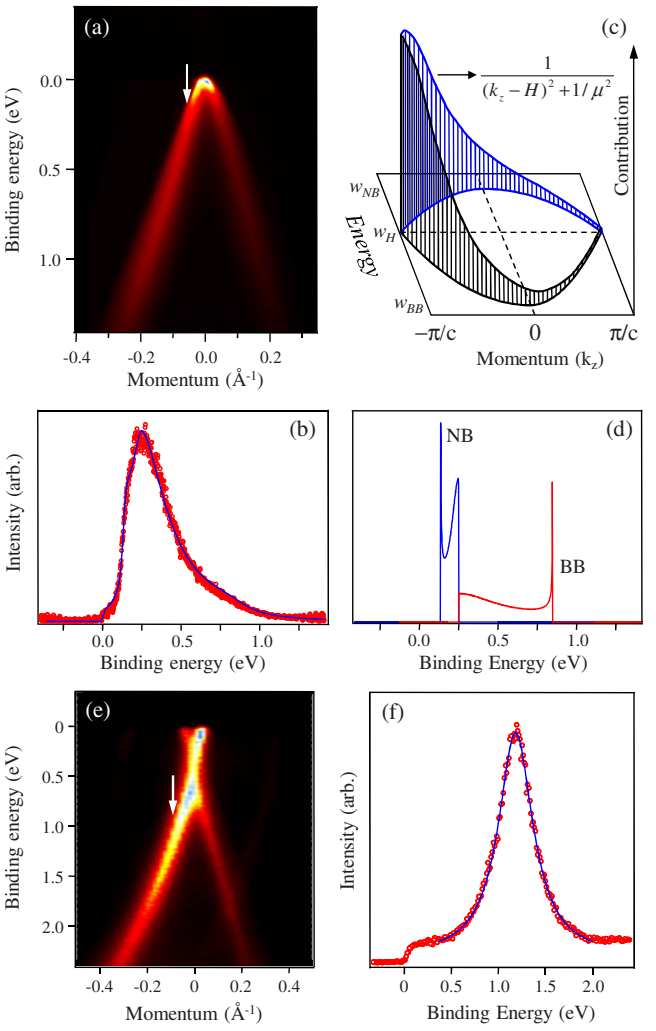

FIG. 4. (Color online) (a) ARPES data taken at *H* point of graphite along *L*-*H*-*A* direction. (b) The EDC at the *k* point marked the arrow in panel (a). Circles are the experimental data and thick line is the fit for which finite escape depth effect in photoemission process has been considered (see the text). (c) Contributions from different k_z points due to the finite escape depth effect. (d) The model fitting function with finite escape effect considered but without lifetime effect. (e) ARPES data at *K* from epitaxially grown graphene on 6*H*-SiC. (f) The EDC [at the *k* point marked by the arrow in panel (e)] shows symmetric line shape unlike that from graphite. The EDCs can be fitted with a single Lorentzian and constant background (thick line).

4(c). As the BB and NB have finite k_z dispersions, the contribution from other k_z values results in broadening of the spectral function. The fact that the BB has more k_z dispersion gives more broadening on the higher-binding-energy side as seen in Fig. 4(b).

Figure 4(d) depicts a model spectral function when all these effects are accounted for. Only when such effects are considered can one extract the true lifetime broadening. We used $\mu=7$ Å for the fitting,[40] and the model function in Fig. 4(d) is convolved with a Fermi function and a Voigt function with the Gaussian width set to the total energy resolution of 40 meV. In addition, we used binding-energy-dependent Lorentzian width for the Voigt function considering the ob-

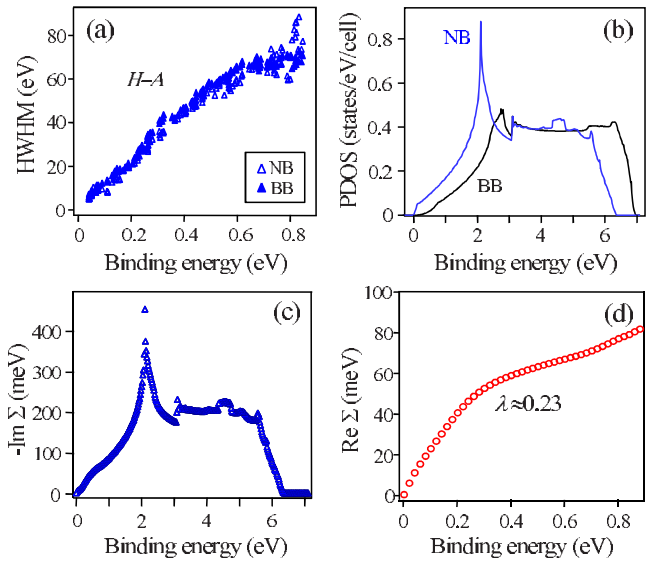

FIG. 5. (Color online) (a) Extracted half-width at half maximum (HWHM) as a function of the binding energy for NB (empty triangles) and BB (filled triangles). (b) Calculated partial electronic densities of states (pDOSs) for NB and BB. (c) Constructed Σ'' from the data in panel (a) for the low-energy region and pDOS in panel (b). pDOS is scaled so that it matches the experimental HWHM at 0.9 eV. (d) Σ' using Hilbert transform of Σ''. The EPC parameter is ≈ 0.23.

servation from the K data that the Lorentzian width linearly increases as a function of binding energy.[14]

Even though this k_z uncertainty is a general property of ARPES measurement, perfect 2D material such as graphene should not show this escape depth effect in its ARPES data because it has no dispersion in the k_z direction. To ensure that the asymmetric line shape in graphite is indeed from the finite escape depth effect, we took graphene ARPES data and checked if the line shape was symmetric as expected. Figure 4(e) shows ARPES data along the M-K-Γ direction of graphene which was epitaxially grown on 6H-SiC. Figure 4(f) is an EDC curve from the k-point arrow marked in panel (e). The EDC shows very symmetric line shape contrary to the EDC in panel (b). One can fit this curve with a single Lorentzian with constant background as shown with the thick line in Fig. 4(f). An almost perfect fit strongly supports the idea that the asymmetric line shape of graphite data is indeed from the finite escape depth effect.

Figure 5(a) shows the half-width at half maximum (HWHM) found by fitting our model to the EDCs along the high-symmetry line H-A. Filled and empty symbols represent BB and NB widths, respectively. There is almost no difference between the BB and NB widths. The width increases linearly as a function of the binding energy. We find that the width shows no high-order dependence such as $\sim\omega^2$. This also indicates that the EPC is the dominant decay channel in graphite as expected from our model. Yet, observation of very weak or no kinky feature at the optical phonon energy of 0.2 eV shows that EPC is very weak in graphite. On the other hand, the width converges to zero as the binding energy goes to zero, which means that momentum mixing due to impurities or defects is minimal, supporting again the high quality of the samples.

One can extract the EPC parameter from the derivative of Σ' at $\omega=0$. Conventionally, one obtains the Σ' from the difference between the experimental dispersion and the bare band. In graphite, this is a difficult task because the bare band may not be linear. On the other hand, even though harder, one can get Σ' by Hilbert transforming Σ''. To do the Hilbert transformation, we need to know Σ'' over the entire energy range. As this is not the case, we use scaled partial electronic density of states (pDOS) as Σ'', assuming that Σ'' is approximately proportional to pDOS.[14] Figure 5(b) shows pDOSs of NB and BB. Figure 5(c) is the Σ'' for the NB, obtained from the experimental data and calculated pDOS for the NB. The Hilbert transform of it gives the Σ' shown in Fig. 5(d). According to Eq. (5), we can find the electron-phonon coupling parameter from the energy derivative of Σ' at $\omega=0$. The resulting value is $\lambda \approx 0.23$, very similar to the value of $\lambda=0.2$ for the K-Γ direction reported in our previous work.[14] This value is larger than the calculated value of 0.075 for graphene[7] but much smaller than the previously reported value for graphite.[13] In addition, this value is consistent with the value of 0.21 calculated with a reasonable scattering amplitude g.[9] Therefore, we conclude that EPC constant λ is also small at the H point.

B. Finite-temperature case

Figure 6 shows temperature-dependent ARPES data at the K point of graphite, which were taken at 225, 175, 125, 75, and 25 K. One can clearly distinguish the NB from the BB in each panel. Note that the binding-energy difference between the NB and the BB is about 0.8 eV. Overall, the data do not appear to show much temperature dependence. To see this quantitatively, we performed the same line-shape analysis we developed on the data. Every EDC from −0.2 to 0 Å of each panel in Fig. 6 is fitted with our model function and HWHM is extracted.

Extracted HWHM vs binding energy at different temperatures is plotted in Fig. 7. Overall, HWHMs linearly increase proportionally to binding energy. All HWHMs are quite similar to each other, and one can safely say that there is no clear temperature evolution of the spectral function. This already indicates that the energy of the phonon mode which is involved in electron-phonon coupling in graphite is very high compared to the temperature scale of our measurement (225 K).

The calculated imaginary part of the self-energy is used to fit the extracted HWHM of the 25 K data [Fig. 8(a)]. In fitting the data, we assumed an Einstein phonon of $\omega_0 = 200$ meV. The imaginary part is supplemented with a constant plus an energy-dependent term, $\Sigma_{ee}=A\omega^2$, in order to simulate the electron-electron interactions. The partial DOS of the NB band were calculated from the local-density approximation (LDA) calculation. The coupling amplitude g is a fitting parameter. We find that g is ≈ 0.39 eV and the electron-electron interaction prefactor is ≈ 0.004. Note that negligible electron-electron interaction near the Fermi energy is confirmed as predicted earlier in our model.

With the fit result, one may try to evaluate the electron-phonon coupling constant λ from the g value. By Hilbert

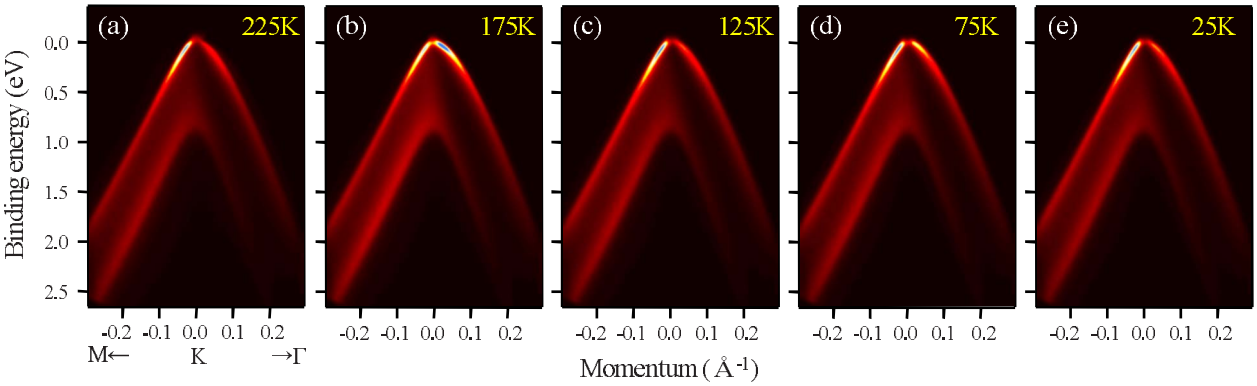

FIG. 6. (Color online) ARPES data taken along M-K-Γ at different temperatures. (a), (b), (c), (d), and (e) were taken at 225, 175, 125, 75, and 25 K, respectively.

transforming the model fit function of Σ'', we obtain Σ'. The derivative of Σ' at $\omega=0$ as in Eq. (4) gives us λ of ≈ 0.14. This value is smaller than the value of $\lambda=0.2$ at K which was obtained from the experimental data.[14] A key difference between the two methods is that while we assume an Einstein phonon of $\omega=200$ meV, no such assumption is used in transforming the experimental data. However, the experimental data are more susceptible to systematic errors, especially at very low binding energy range (where the line shape is affected by Fermi function). Since the low-energy range has more effect on λ and a theoretical result shows that $\omega=200$ meV is the dominant phonon,[7] $\lambda=0.2$ probably gives us the upper bound for the electron-phonon coupling.

Other panels in Fig. 8 show HWHMs and fitted model function at different temperatures. The fitting was conducted on NB along M-K near the Fermi energy at each temperature. As could already been seen in Fig. 7, fitting of the HWHM results in negligible temperature dependence. This indicates that the phonon involved in the coupling has a much higher energy scale than 225 K. In fact, the 200 meV bond-stretching mode may be the most dominant one as the *ab initio* calculation on graphene shows.[7]

V. CONCLUSION

We present high-resolution ARPES data taken at the H point of natural graphite single crystals. The graphite bands show a linear dispersion as predicted in LDA calculation and the NB and BB are degenerate. First, we considered various scattering mechanisms in graphite. We deduced a theoretical formula for the scattering rate by phonons. We find that the scattering rate by EPC increases linearly with binding energy due to the linear density of states. Electron-electron interactions in graphite are negligible in the low binding energy region where the band dispersion is linear. The impurity or defect scattering rate is also proportional to binding energy because of linear DOS. We show that all effects other than phonon scattering are negligible. Second, with the finite escape depth effect in the photoemission process considered, we extracted Σ'' from the EDCs of the NB and BB separately. Finally, we approximated Σ'' by combining the experimental HWHM Σ'' and calculated partial DOS. The obtained Σ'' is converted to Σ' through a Hilbert transform. The extracted EPC parameter at H is ≈ 0.23, which is small, consistent with the value of 0.2 from the K point in our previous

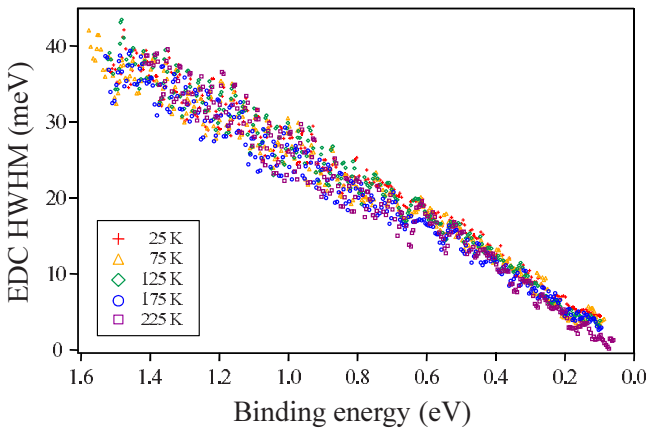

FIG. 7. (Color online) HWHM vs binding energy at different temperatures: 25, 75, 125, 175, and 225 K. HWHM is extracted from NB band along M-K near Fermi energy.

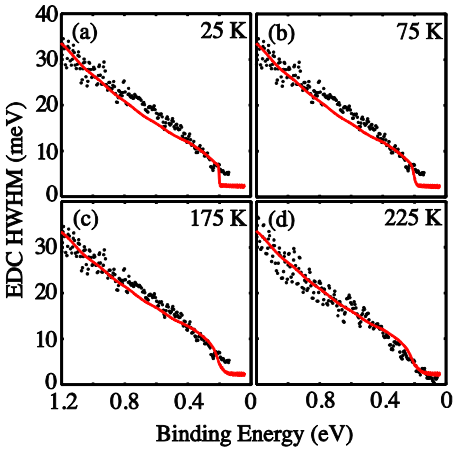

FIG. 8. (Color online) HWHMs extracted from ARPES data at different temperatures are fitted by calculated imaginary part of self-energy. Panels (a), (b), (c), and (d) are for temperatures of 25, 75, 125, and 175 K, respectively. The solid line in each panel is the best fit to the experimental data by calculated imaginary part of self-energy. The calculated imaginary part of self-energy includes electron-phonon and electron-electron interaction terms. The electron-phonon coupling constant and electron-electron interaction prefactor were used as fitting parameters (see the text).

work. This small EPC parameter is also consistent with very weak kinky features in our data.

In addition, we conducted temperature-dependent ARPES measurements on the graphite *K* point. The temperature-dependent data show no notable evolution in the EDC line shape within the temperature range (25–225 K). Analyzing the experimental temperature dependence of peak widths and simulated temperature dependence, we conclude that the dominant phonon mode in EPC in graphite is much larger than the temperature scale of our experiment (225 K). This is consistent with the notion that the phonon mode in electron-phonon coupling in graphite is the 200 meV optical phonon mode, as is the case for graphene.

Even though electron-phonon coupling has been heavily studied, most of these studies were focused on metallic systems where the density of states near the Fermi level is approximately constant. Such is not generally true, especially for semimetals. The formulas discussed in this work are very general and can be used for any shape of electronic density of states. It should therefore be useful in future studies on semimetals.

ACKNOWLEDGMENTS

The authors acknowledge fruitful discussions with J. H. Han. This work was supported by the KICOS under Grant No. K20602000008. C.S.L. acknowledges support through the BK21 Project and helpful discussions with J.-W. Rhim. H.J.C. acknowledges support from the KRF (Grant No. KRF-2007-314-C00075), the KOSEF (Grant No. R01-2007-000-20922-0), and the KISTI Supercomputing Center (Grant No. KSC-2008-S02-0004). ALS is operated by the Office of BES of DOE.

*cykim@phya.yonsei.ac.kr

[1] L. D. Landau, Sov. Phys. JETP **3**, 920 (1957).
[2] S. Xu, J. Cao, C. C. Miller, D. A. Mantell, R. J. D. Miller, and Y. Gao, Phys. Rev. Lett. **76**, 483 (1996).
[3] G. Moos, C. Gahl, R. Fasel, M. Wolf, and T. Hertel, Phys. Rev. Lett. **87**, 267402 (2001).
[4] J. González, F. Guinea, and M. A. H. Vozmediano, Phys. Rev. Lett. **77**, 3589 (1996).
[5] C. D. Spataru, M. A. Cazalilla, A. Rubio, L. X. Benedict, P. M. Echenique, and S. G. Louie, Phys. Rev. Lett. **87**, 246405 (2001).
[6] G. Grimvall, in *The Electron-Phonon Interaction in Metals*, Selected Topics in Solid State Physics, edited by E. Wohlfarth (North-Holland, New York, 1981).
[7] C.-H. Park, F. Giustino, M. L. Cohen, and S. G. Louie, Phys. Rev. Lett. **99**, 086804 (2007).
[8] M. Calandra and F. Mauri, Phys. Rev. B **76**, 205411 (2007).
[9] J. D. Lee, S. W. Han, and J. Inoue, Phys. Rev. Lett. **100**, 216801 (2008).
[10] F. Tuinstra and J. L. Koenig, J. Chem. Phys. **53**, 1126 (1970).
[11] J. Maultzsch, S. Reich, C. Thomsen, H. Requardt, and P. Ordejón, Phys. Rev. Lett. **92**, 075501 (2004).
[12] M. Mohr, J. Maultzsch, E. Dobardžić, S. Reich, I. Milošević, M. Damnjanović, A. Bosak, M. Krisch, and C. Thomsen, Phys. Rev. B **76**, 035439 (2007).
[13] K. Sugawara, T. Sato, S. Souma, T. Takahashi, and H. Suematsu, Phys. Rev. Lett. **98**, 036801 (2007).
[14] C. S. Leem, B, J. Kim, Chul Kim, S. R. Park, T. Ohta, A. Bostwick, E. Rotenberg, H.-D. Kim, M. K. Kim, H. J. Choi, and C. Kim, Phys. Rev. Lett. **100**, 016802 (2008).
[15] A. Bostwick, T. Ohta, T. Seyller, K. Horn, and E. Rotenberg, Nat. Phys. **3**, 36 (2007).
[16] J. W. McClure, Phys. Rev. **108**, 612 (1957).
[17] J. C. Slonczewski and P. R. Weiss, Phys. Rev. **109**, 272 (1958).
[18] A. Zunger, Phys. Rev. B **17**, 626 (1978).
[19] R. C. Tatar and S. Rabii, Phys. Rev. B **25**, 4126 (1982).
[20] J. C. Charlier, J. P. Michenaud, and X. Gonze, Phys. Rev. B **46**, 4531 (1992).
[21] A. R. Law, J. J. Barry, and H. P. Hughes, Phys. Rev. B **28**, 5332(R) (1983).
[22] T. Takahashi, H. Tokailin, and T. Sagawa, Phys. Rev. B **32**, 8317 (1985).
[23] A. R. Law, M. T. Johnson, and H. P. Hughes, Phys. Rev. B **34**, 4289 (1986).
[24] I. R. Collins, P. T. Andrews, and A. R. Law, Phys. Rev. B **38**, 13348 (1988).
[25] F. Maeda, T. Takahashi, H. Ohsawa, S. Suzuki, and H. Suematsu, Phys. Rev. B **37**, 4482 (1988).
[26] M. Vos, P. Storer, S. A. Canney, A. S. Kheifets, I. E. McCarthy, and E. Weigold, Phys. Rev. B **50**, 5635 (1994).
[27] E. L. Shirley, L. J. Terminello, A. Santoni, and F. J. Himpsel, Phys. Rev. B **51**, 13614 (1995).
[28] C. Heske, R. Treusch, F. J. Himpsel, S. Kakar, L. J. Terminello, H. J. Weyer, and E. L. Shirley, Phys. Rev. B **59**, 4680 (1999).
[29] V. N. Strocov, A. Charrier, J. M. Themlin, M. Rohlfing, R. Claessen, N. Barrett, J. Avila, J. Sanchez, and M. C. Asensio, Phys. Rev. B **64**, 075105 (2001).
[30] T. Kihlgren, T. Balasubramanian, L. Walldén, and R. Yakimova, Phys. Rev. B **66**, 235422 (2002).
[31] S. Y. Zhou, G. H. Gweon, C. D. Spataru, J. Graf, D. H. Lee, S. G. Louie, and A. Lanzara, Phys. Rev. B **71**, 161403(R) (2005).
[32] K. Sugawara, T. Sato, S. Souma, T. Takahashi, and H. Suematsu, Phys. Rev. B **73**, 045124 (2006).
[33] S. Y. Zhou, G.-H. Gweon, J. Graf, A. V. Fedorov, C. D. Spataru, R. D. Diehl, Y. Kopelevich, D.-H. Lee, Steven G. Louie, and A. Lanzara, Nat. Phys. **2**, 595 (2006).
[34] S. Y. Zhou, G. H. Gweon, and A. Lanzara, Ann. Phys. **321**, 1730 (2006).
[35] D. Binosi and L. Theußl, Comput. Phys. Commun. **161**, 76 (2004).
[36] G. D. Mahan, *Many-Particle Physics*, 3rd ed. (Kluwer Academic/Plenum, New York, 2000).
[37] B. Feuerbacher and B. Fitton, Phys. Rev. Lett. **26**, 840 (1971).
[38] T. Balasubramanian, E. Jensen, X. L. Wu, and S. L. Hulbert, Phys. Rev. B **57**, R6866 (1998).
[39] T. Ohta, A. Bostwick, T. Seyller, K. Horn, and E. Rotenberg, Science **313**, 951 (2006).
[40] S. Tanuma, C. J. Powell, and D. R. Penn, Surf. Interface Anal. **17**, 911 (1991).